Journal of Alloys and Compounds 580 (2013) 15–22

Contents lists available at SciVerse ScienceDirect

Journal of Alloys and Compounds

journal homepage: www.elsevier.com/locate/jalcom

Low-temperature synthesis of alkalis doped TiO_2 photocatalysts and their photocatalytic performance for degradation of methyl orange

Guidong Yang [a,c,*], Zifeng Yan [b], Tiancun Xiao [c], Bolun Yang [a]

[a] Department of Chemical Engineering, School of Chemical Engineering and Technology, Xi'an Jiaotong University, Xi'an 710049, China
[b] State Key Laboratory for Heavy Oil Processing, China University of Petroleum, Qingdao 266555, China
[c] Department of Chemistry, Inorganic Chemistry Laboratory, University of Oxford, Oxford OX1 3QR, UK

ARTICLE INFO

Article history:
Received 15 March 2013
Received in revised form 6 May 2013
Accepted 12 May 2013
Available online 20 May 2013

Keywords:
Alkali ion doping
Solvothermal synthesis
TiO_2
Photocatalytic
Degradation

ABSTRACT

In this study, a series of alkalis doped TiO_2 (alkalis = Na, K and Rb) photocatalysts were synthesized at low temperature using solvothermal method. Various characterization techniques, such as X-ray diffraction (XRD), Raman spectroscopy, Fourier transform infrared spectra (FT-IR), Scanning electron microscopy (SEM), N_2 adsorption and UV–vis diffuse reflectance spectra (DRS) spectrophotometer, were employed to investigate the influence of alkali ions on the crystalline phase, grain size, optical absorption and surface functional groups of alkali ion doped TiO_2 catalysts. The XRD results indicate that the alkali ion doping restrains the growth of the TiO_2 particle size, resulting in a high specific surface area for the alkali ion doped TiO_2 materials. The photocatalytic performances of these materials were evaluated using the degradation of methyl orange (10 mg/L) as the model reaction under UV light irradiation. It was found that the photocatalytic activity of the alkali ion doped TiO_2 catalysts can be enhanced significantly with the samples doped by 3 wt% alkali ion, which is due to the synergistic effect of pure anatase TiO_2 phase structure, small crystallite size, higher surface basic sites and fast electronic transfer rate.

1. Introduction

Titanium dioxide (TiO_2) is a well-known semiconductor with a broad band gap, which has attracted much attention because of their outstanding chemical and thermal stability, high refractive index, great ultraviolet absorptivity, and resistance to photocorrosion [1–6]. Some potential applications of TiO_2 have been developed in various fields, including photocatalytic water splitting, environmental purification, self-cleaning and microorganism photolysis [1–9]. There are three polymorphs of TiO_2 existing naturally: rutile, anatase and brookite [10]. While rutile is the most thermodynamically stable bulk phase, the anatase structure has been extensively investigated in many studies, which demonstrated that the anatase phase has higher photocatalytic activity than rutile and is often dominant in nanocrystalline TiO_2, due to its lower surface energy than rutlie [10,11]. However, the major drawback to the widespread use of anatase TiO_2 as photocatalysts is its relatively lower photocatalytic efficiency [12,13], which is due to the quick recombination of photoinduced charge carriers in the application of environmental protection.

In order to improve the photocatalytic efficiency, modifications of TiO_2 have been explored to promote the separation of the electron–hole pairs during the photocatalytic reaction, and many studies reported the photocatalytic activity enhancement in the decomposition of organic pollutants by various synthesized approaches [12–16]. More recently, chemical promotion of catalytic materials by alkalis has been a subject of many investigations [17–21]. Bessekhouad et al. [18] reported that the alkalis modified titanium dioxide prepared using sol–gel and impregnation method gives a higher activity than that of P25 TiO_2. This effect was attributed to the alkalis doping could improve electron transfer efficiency, consequently increasing the amount of produced radicals. López et al. [19] found that Li/TiO_2 and Rb/TiO_2 synthesized by sol–gel method possesses high surface areas, which approached to 100 m^2/g when they are annealed at temperatures of 400 °C. Bouattour et al. [20] demonstrated that the Rb^+ and (Rb^+, Y^{3+}) doped and codoped TiO_2 samples showed a great enhancement in the photocatalytic efficiency for the degradation of 2-naphthol under sunlight irradiation. In addition, Panagiotopoulou and Kondarides [21] found that adding a small amount of alkalis (x = Li, Na, K, Cs) to TiO_2 resulted in the reduction of Ti^{4+} surface species and created a new type of sites at the perimeter of the dispersed metal crystallites, which provide the necessary dual-function sites required for the water–gas shift reaction to proceed. These studies showed that alkalis modification had a strong promotional effect in the performance of TiO_2, which is often observed

* Corresponding author at: Department of Chemical Engineering, School of Chemical Engineering and Technology, Xi'an Jiaotong University, Xi'an 710049, China.
E-mail addresses: guidongyang@mail.xjtu.edu.cn (G. Yang), Xiao.tiancun@chem.ox.ac.uk (T. Xiao).

0925-8388/$ - see front matter © 2013 Elsevier B.V. All rights reserved.
http://dx.doi.org/10.1016/j.jallcom.2013.05.074

in the enhanced photocatalytic activity and improvement of visible light absorption. However, a systematical study on the effect of alkali ions doping on the photocatalytic performances of TiO_2 has not been reported so far.

In recent years, the preparation of functional metal oxides using low-energy and environmentally benign processes has received much attention [22–24]. Here, a facile solvothermal method has been adopted to prepare alkalis doped TiO_2 with highly crystalline anatase phase, which is considered to be essential for photoactive catalysis. The prepared TiO_2 materials are characterized using X-ray diffraction (XRD), Raman spectroscopy, Fourier transform infrared spectra (FT-IR), Scanning electron microscopy (SEM), N_2 adsorption and UV–vis diffuse reflectance spectra (DRS) spectrophotometer. Moreover, the photocatalytic characteristics of the as-prepared alkalis doped TiO_2 samples are evaluated by measuring the degradation of MO and compared with those of the pure TiO_2 sample.

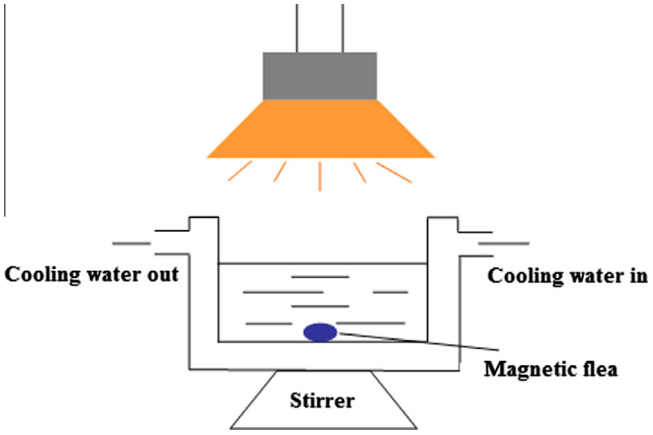

Fig. 1. The schematic diagram of photocatalytic activity testing.

2. Experimental section

2.1. Catalyst preparation

A series of alkalis doped TiO_2 (alkalis = Na, K and Rb) photocatalysts were prepared using solvothermal method. Tetrabutyl orthotitanate ($C_{16}H_{36}O_4Ti$, Sigma–Aldrich) was used as titanium source. Alkali metal nitrates (Na, K, Rb) was used as the precursor of doped metal oxides. In a typical synthesis procedure, 0.01 mol tetrabutyl orthotitanate was dispersed in 10 mL absolute ethanol to give a solution which was then slightly stirred for 30 min to form solution A. The required amounts of nitrate precursors (from 1 wt% to 5 wt%) were dissolved to a 50 mL beaker containing 20 mL absolute ethanol and the resulting mixture was stirred for 30 min to form solution B. During the stirring, 1.0 mL of acetic acid and deionized water were added into the solution B. Afterwards, the two solutions were mixed for 30 min and heated in a Teflon-lined stainless steel autoclave and kept 110 °C for 24 h. The heated solution was removed from oven and allowed to cool to room temperature naturally. The as-synthesized products were filtrated and washed with ethanol and deionized water, respectively, and then dried in an oven at 80 °C overnight. The resultant samples were then annealed at 400 °C for 3 h in air to give the final alkalis doped TiO_2 samples. The obtained nanoparticle samples were labeled M–TiO_2-x% (M = Na, K, Rb and x = 1, 3, 5). The pure TiO_2 nanocrystal was prepared by the same procedure without adding the alkalis precursor and used here as a reference sample.

2.2. Characterizations of the materials

The crystalline structure and crystallite size of the resulting alkalis doped TiO_2 materials were determined using X-ray diffraction with a Philips X′ PeRT Pro Alpha 1 diffractometer with Cu Kα radiation (λ = 1.5406 Å) operated at a tube current of 40 mA and a voltage of 45 kV. Data were collected over 2θ values from 10° to 80°, at a scan speed of 1° min^{-1}. The average crystallite size was calculated using Scherrer equation: $d = 0.9\lambda/b(2\theta)\cos\theta$, where $b(2\theta)$ is the width of the strongest XRD peak of anatase (101) TiO_2 at half peak-height in radian (FWHM), λ is the wavelength (nm) of the monochromatic X-ray beam, θ is the angle between the incident and diffracted beams in degree, and d is the average crystallite size of the as-prepared powder sample in nanometer. The UV–vis diffuse reflectance spectra were obtained using a Perkin Elmer Lambda 750S UV/Vis spectrometer equipped with an integrating sphere assembly. The spectra were recorded at room temperature in air from 320 to 520 nm. The geometry and morphology of the alkalis doped TiO_2 materials were investigated by JSM840F scanning electron microscopy (SEM). Laser Raman spectra were recorded using a Perkin Elmer 400F Ramanstation Raman spectrometer. Fourier transform infrared (FT-IR) spectra were carried out by diffused reflectance using a Bruker Vertex-70. The BET specific surface area of the alkalis doped TiO_2 materials were determined using a N_2 physisorption technique, the samples was degassed at 200 °C overnight before the actual measurement.

2.3. Photocatalytic activity testing

Methyl orange (MO) is a representative dye in aqueous solutions and widely used in various industrial applications, which causes severe environmental problems. In this work, the photocatalytic activities of the alkalis doped TiO_2 samples were evaluated by photodegradation of MO under UV light illumination. Photocatalytic reactions were conducted in an open reactor with a cooling-water-cycle system keeping the reaction temperature constant (see Fig. 1). UV illumination was performed with a 300 W Xenon lamp (Beijing Trusttech, PLS-SXE300). Typically, 100 mg of catalyst and 100 mL of MO aqueous solution (10 mg/L) were added into the reaction system. All of suspensions were magnetically stirred in dark for 120 min to ensure the establishment of adsorption/desorption equilibrium of MO before the irradiation. After 60 min irradiation, the light source was switched off; 3 mL of the solution was taken out and centrifuged to remove the catalysts. The remaining transparent liquid was analyzed in an UV–vis spectrophotometer, and the characteristic absorption peak of MO at 505 nm was used to determine the degradation extent of MO. The efficiency of degradation was calculated using the following formula:

$$\text{MO degradation}\,(\%) : X_{MO} = (C_o - C)/C_o \times 100\%$$

where C_o and C are the original MO solution concentration after the adsorption/desorption reached equilibrium and residual MO concentration after each photoreaction. It should be noted that no sacrificial agent and oxygen were added into the solution during the reaction process.

3. Results and discussion

3.1. Structural characterization

X-ray diffraction (XRD) has the advantage of being a fairly standard laboratory technique which identifies the crystalline structure and phase composition in nanocrysalline materials. Fig. 2 shows the X-ray diffraction patterns of the as-prepared alkalis doped TiO_2 samples with varying nitrates precursor doping level and these samples are annealed at 400 °C for 3 h. For the comparison, the XRD data of the M–TiO_2-1% samples obtained after solvothermal reaction at 110 °C for 24 h are also shown in Fig. 2, and these three samples were measured without calcinations. It can be seen that although the crystallization temperature of the solvothermal treatment was as low as 110 °C, well-crystallized anatase titanium was observed in the no-annealing M–TiO_2-1% samples, indicating that the synthesis method is effective for the preparation of TiO_2 nanocrystals even at low temperature. As shown in Fig. 2, the crystal structure of the as-prepared Na–TiO_2, K–TiO_2 and Rb–TiO_2 samples obtained after calcination is quite similar, which has a single phase of TiO_2 crystals with tetragonal anatase structure, and no other impurity peaks are observed in these samples. These results indicate that the alkali ions either have entered into the TiO_2 lattice under our solvothermal conditions, or they might be highly dispersed in the high surface TiO_2, which is not detectable using XRD. For the Na–TiO_2 and K–TiO_2 sample, with the increase of calcinations temperature, the XRD patterns demonstrate the main (101) Bragg peak of annealed alkalis doped TiO_2 become sharper and more intense, suggesting that the formation of higher crystallinity for doped TiO_2 and the presence of amorphous phase has been transformed to anatase phase during calcinations. In contrast, the XRD pattern of Rb–TiO_2 shown in Fig. 2c exhibits that the intensity of Rb-TiO_2 diffraction peaks have no significant changes after calcinations, implying that

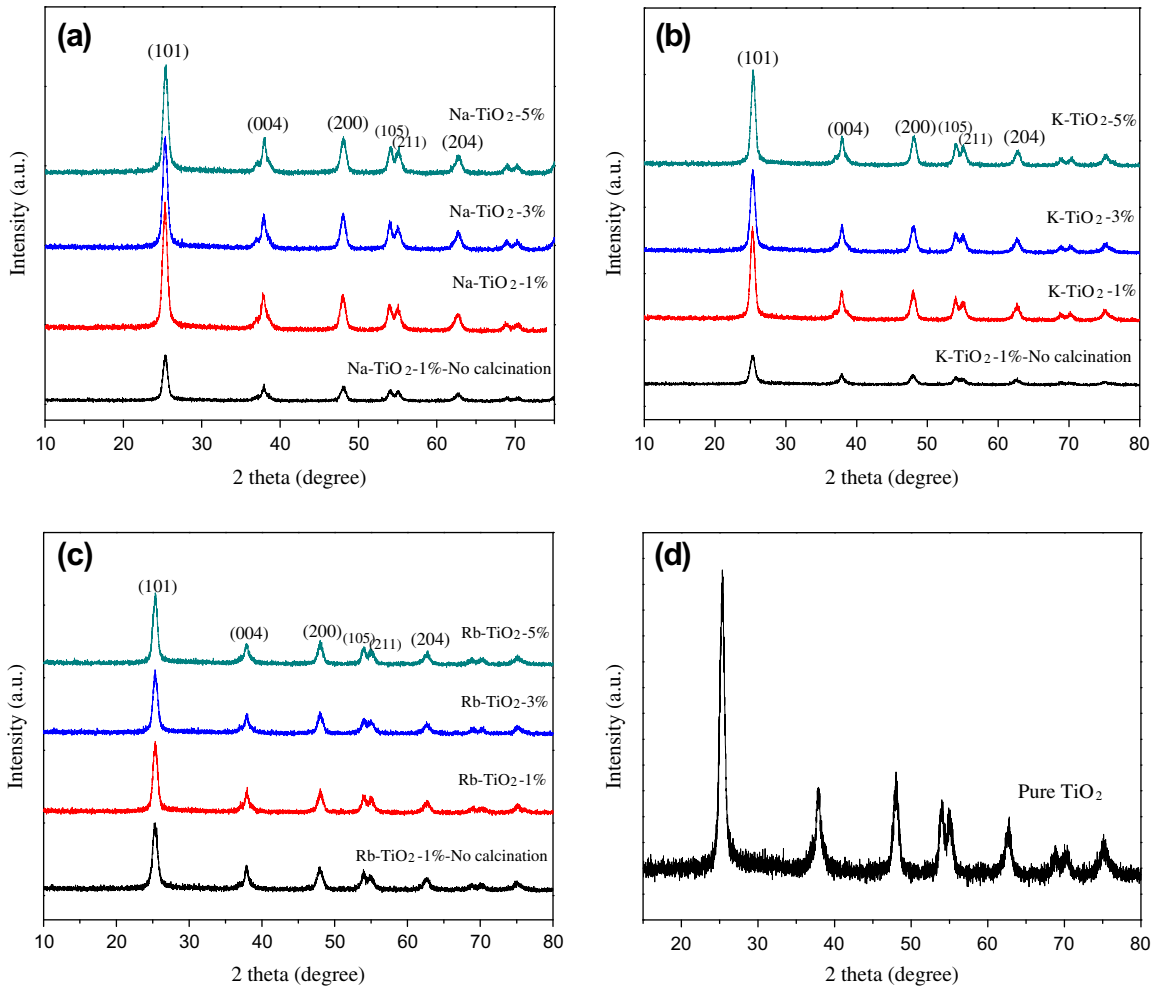

Fig. 2. XRD patterns of alkalis doped TiO_2 samples and pure TiO_2. All the samples were annealed at 400 °C for 3 h.

further increase of annealing temperature to 400 °C cannot affect the crystallization degree of Rb–TiO_2 samples.

Table 1 lists the average crystallite sizes of the material particles determined with the XRD peak broadening analysis using the Scherrer formula. It was shown that the crystallite size of alkalis doped TiO_2 is in the range of 10–36 nm, which are all smaller than that of the reference pure TiO_2 sample except the K–TiO_2-1% sample. In addition, the enlarged localized profile of main (101) Bragg peaks around at 2θ of 25.3° in Fig. S1 reveals that the K–TiO_2 and Rb–TiO_2 samples prepared with 3 wt% alkali ions doping have an obviously broader anatase (101) diffraction peak than the samples doped with 1 wt% and 5 wt% alkali ions. As listed in Table 1, the FWHM value of K–TiO_2-3% and Rb–TiO_2-3% is 0.845 and 0.922, respectively, which corresponds to smaller crystallite size values. Further, the calculation result listed in Table 1 also suggests that the K–TiO_2-3% and Rb–TiO_2-3% have the smallest crystallite sizes, which are 9.6 and 8.8 nm, respectively. This may be due to that the alkali ions penetrated into TiO_2 lattice, or they probably are bonded with oxygen onto TiO_2 surface to form alkalis oxides, both of the two factors restricted the growth of TiO_2 nanocrystal [18,19]. The BET surface areas of the Na–TiO_2-3%, K–TiO_2-3% and Rb–TiO_2-3% photocatalysts were also given in Table 1. It

Table 1
FWHM, crystallite size, phase composition, BET surface area, energy band gap and photoactivities[a] of alkalis doped TiO_2 and pure TiO_2 samples.

Samples	Doping level	FWHM	Crystallite size (nm)	Phase composition	BET (m^2/g)	E_g (eV)	Degradation yield (%)
Pure TiO_2	0	0.259	31.3	Anatase	39.23	3.19	65
	1 wt%	0.461	17.7	Anatase	–	3.19	73
Na–TiO_2	3 wt%	0.307	26.5	Anatase	46.5	3.19	77
	5 wt%	0.307	26.5	Anatase	–	3.17	32
	1 wt%	0.234	35.3	Anatase	–	3.20	56
K-TiO_2	3 wt%	0.845	9.6	Anatase	51.61	3.20	70
	5 wt%	0.269	30.3	Anatase	–	3.19	66
	1 wt%	0.346	23.5	Anatase	–	3.20	58
Rb-TiO_2	3 wt%	0.922	8.8	Anatase	50.52	3.19	66
	5 wt%	0.384	21.2	Anatase	–	3.21	63

[a] Reaction conditions: 0.10 g of photocatalyst, 100 ml 10 mg/L methyl orange(MO) aqueous solution, a 300 W Xe lamp at 15 cm away from the reaction solution, reaction temperature = 303 K, stirring rate = 700 rpm, reaction period = 60 min.

can be found that the BET surface areas of the alkalis doped TiO_2 samples are much similar in the range of 46–52 m^2/g, and all of them show larger specific surface areas in comparison with pure TiO_2 sample.

The crystalline structure and phase components of alkalis doped TiO_2 samples are further confirmed by Raman spectroscopy. Fig. 3 shows the Laser Raman spectra of alkalis doped TiO_2, including data for the no-annealing samples for comparison. It can be observed that the main features of the Raman spectra of all alkalis doped TiO_2 photocatalysts as well as the no-annealing TiO_2 samples are very similar: there are six characteristic bands at 144 cm^{-1} (E_g), 197 cm^{-1} (E_g), 399 cm^{-1} (B_{1g}), 513 cm^{-1} (A_{1g}), 519 cm^{-1} (B_{1g}) and 639 cm^{-1} (E_g) seen in the Raman spectra, which correspond to the anatase phase [25–27], with no peaks due to the rutile phase appeared. This suggested that well-crystalline TiO_2 particles can be formed at a lower temperature under our experimental conditions. These findings are in agreement with the XRD analysis. The inset of Fig. 3 shows the localized profile of main Raman peak (E_g) range from 120 cm^{-1} to 220 cm^{-1}, which can provide more information of phase evolution of the catalyst materials. Comparing with the Raman spectra of no-annealing samples, it is obvious that the principal Raman peaks of Na–TiO_2, K–TiO_2 and Rb–TiO_2 nanoparticles shifts towards lower Raman shift after direct calcinations at 400 °C for 3 h, indicating that the crystal particles of alkalis doped TiO_2 samples grow up due to a sintering effect [17]. It is worthy of noting that the intensity of the E_g, B_{1g} and A_{1g} band for Na–TiO_2 , K–TiO_2 and Rb–TiO_2 samples become more broadening and intense after calcinations at 400 °C, indicating a higher crystalline of the doped TiO_2 samples.

Fig. 4 shows the corresponding UV–vis diffuse reflectance spectra of the alkalis doped TiO_2 samples with various alkali ions doping content, including the data for the pure TiO_2, used here as a reference. As shown in Fig. 4, there are no significant optical property difference between the doped TiO_2 samples and the pure reference TiO_2. The spectra of the synthesized alkalis doped TiO_2 (Na–TiO_2, K–TiO_2 and Rb–TiO_2) and undoped TiO_2 show a strong and broad absorption feature in the UV region (below 380 nm) due to the inter band electronic transitions [28,29]. In addition, it can be observed that the absorption edge of alkalis doped TiO_2 samples, which were calcined at 400 °C for 3 h, shifts to shorter wavelengths direction compared to that of undoped TiO_2, particularly in the K–TiO_2 and Rb–TiO_2 samples. This result suggested that the alkali ions doping affects the band gap of TiO_2 to some extent. It is known that the band gap of TiO_2 can be calculated by extrapolation of the straight line from the absorption curve to the abscissa

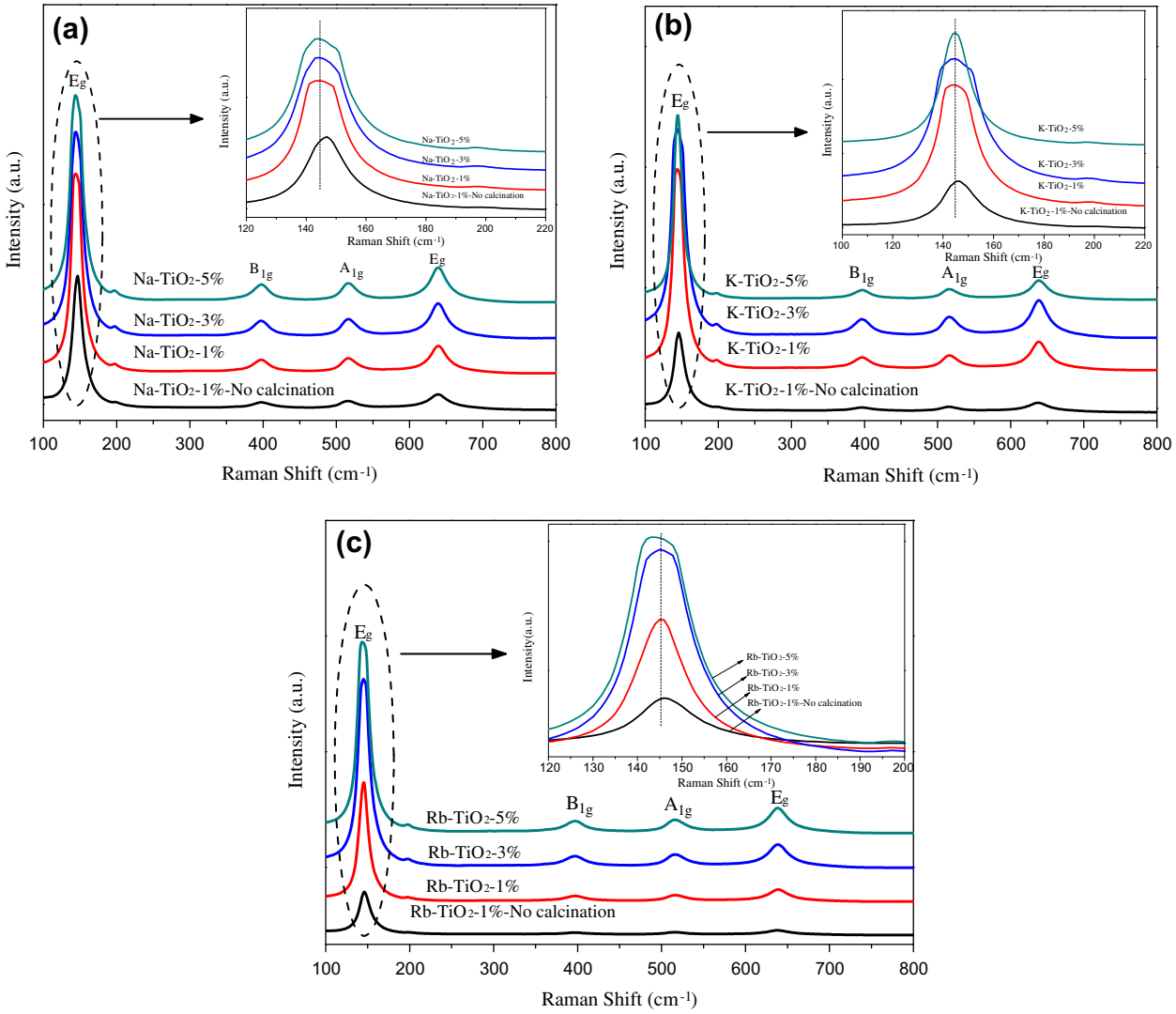

Fig. 3. Laser Raman spectra of alkalis doped TiO_2 samples, the inset of each image is the enlarged localized profile of alkalis doped TiO_2 samples.

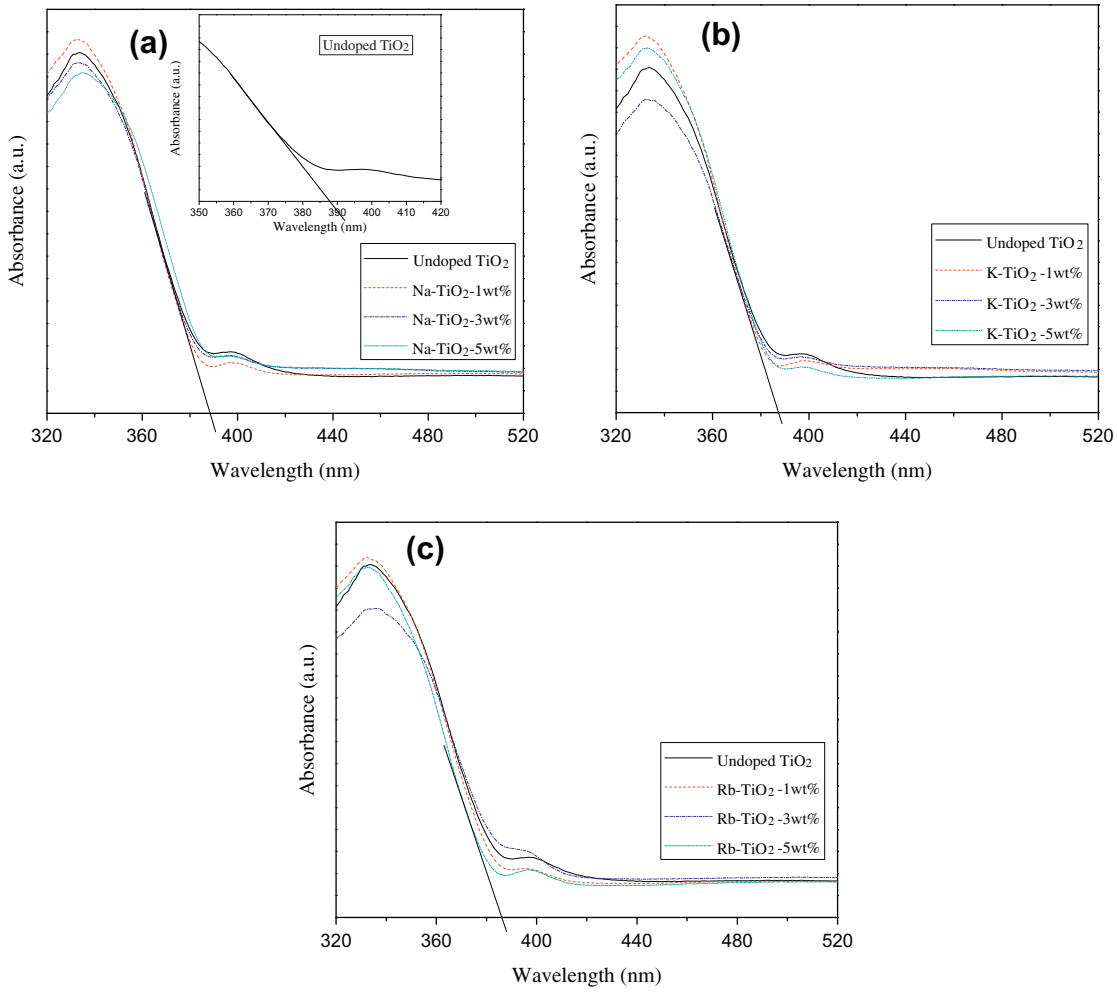

Fig. 4. UV–vis diffuse reflectance spectra of alkalis doped TiO_2 samples, the inset of (a) shows the enlarged localized profile of undoped TiO_2.

from UV–vis absorbance spectra [19]. According to this method, the energy band gap (E_g) for all of alkali ions doped TiO_2 samples is estimated and listed in Table 1. Noted that the band gap of the Rb–TiO_2-5% and Rb–TiO_2-1% were estimated to be 3.21 and 3.20 eV, respectively, this corresponds to 0.02 and 0.01 eV blue shift from the bulk-phase band gap for undoped anatase TiO_2 (3.19 eV), whilst a slight blue shift of energy band gap in the K–TiO_2-3% and K–TiO_2-1% samples (3.20 eV) has also been observed. As previously reported [30,31], the optical band edge of TiO_2 sample exhibits a slight blue shift due to the change of the energy gap of the disorder crystal in TiO_2. On the other hand, it was also reported that the absorption edge exhibits a blue shift due to the quantum size effects [32]. When alkali ions were incorporated into the lattice of TiO_2, the growth of the particle size for as-prepared photocatalysts could be decreased and thus results in the broadening of the energy gap of TiO_2. As listed in Table 1, the particle size of alkalis doped TiO_2 samples is much smaller than that of pure TiO_2. As a result, the doped TiO_2 nanoparticle energy gap becomes widened with the decrease of particle size and therefore leads to a blue shift of optical absorption edge. From the above analysis, it is believed that the blue shift of optical absorption band edge in the present study is the synergetic results of the change of energy gap of the disorder crystal in TiO_2 and the quantum size effects induced by alkalis doping. Accordingly, the visible light absorption for all of the alkalis doped TiO_2 samples is not observed in the UV–vis absorbance spectra which could be easily understood by considering their big energy band gap, suggesting that all of the obtained alkalis doped TiO_2 samples have no photocatalytic activity under visible light irradiation.

Fig. 5a and c shows the representative low-magnification SEM micrographs of Na–TiO_2-3% and K–TiO_2-3% samples prepared using solvothermal reaction of 110 °C for 24 h and subsequent calcination at 400 °C for 3 h to remove the residual organics. It can be seen that both samples exhibit almost the same morphology, which have the large-scale formation of micrometer-sized flake-shaped or irregular aggregates with 5–10 μm in diameter, and indicating that these agglomerates are composed of a large quantity of solid particle structure. It may be noted that a small amount of dispersed TiO_2 particles coexists with the irregular aggregates. The high-magnification SEM images of Na–TiO_2-3% and K–TiO_2-3% samples were shown in Fig. 5b and d. It is clear that the particle surface of Na–TiO_2 sample is relatively rougher than that of K–TiO_2, but no other significant difference.

The typical SEM image of as-prepared Rb–TiO_2-3% is shown in Fig. 6. As can be seen from the SEM image, the obtained sample is mainly composed of solid powder structure, and some small particles are dispersed on the Rb^+ doped TiO_2 surface. It can be observed that the diameter of the oxide particle agglomeration ranges from 5 to 40 μm. Fig. 6 also shows the energy dispersive X-ray spectra of the surface of Rb–TiO_2-3% sample. The results

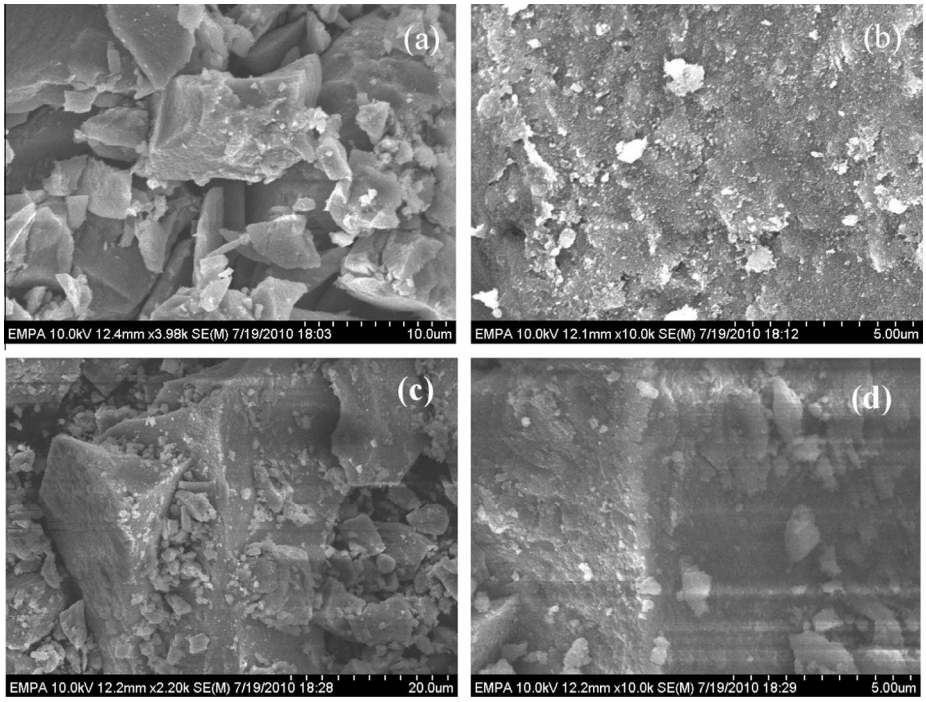

Fig. 5. Representative SEM images of the Na–TiO_2-3% (a and b) and K–TiO_2-3% (c and d) samples with different magnification.

reveal that the C, O and Ti elements coexists over the Rb–TiO_2-3% photocatalysts. In addition to the above elements, the rubidium ions were also detected, indicating that the Rb^+ ions have been present in TiO_2 sample.

Fig. 7 shows the FT-IR spectra of representative alkalis doped TiO_2 and pure TiO_2 samples. The FT-IR spectra reveal that all the as-prepared doped TiO_2 and reference TiO_2 sample exhibit absorbance bands in the range 3700–3100 cm^{-1} indicative of the stretching vibration of –OH or absorbed water molecules [12,14]. The band at 1630 cm^{-1} was attributed to the bending vibrations of the O—H bond, it has been reported that more hydroxyl groups existing on the titania surface favors the enhancement of the photocatalytic activity [33]. The stronger absorbance peak around 800–550 cm^{-1} is corresponding to the vibration of Ti–O and the Ti–O–Ti bridging stretching modes [12,14,34]. In comparison with the pure TiO_2, the alkalis doped TiO_2 samples display one extra absorbance peak at 1350 cm^{-1}, which is assigned to the bending vibration band (υ_3) of nitrate [35], maybe caused by the presence of nitrate species on the surface of obtained TiO_2 sample.

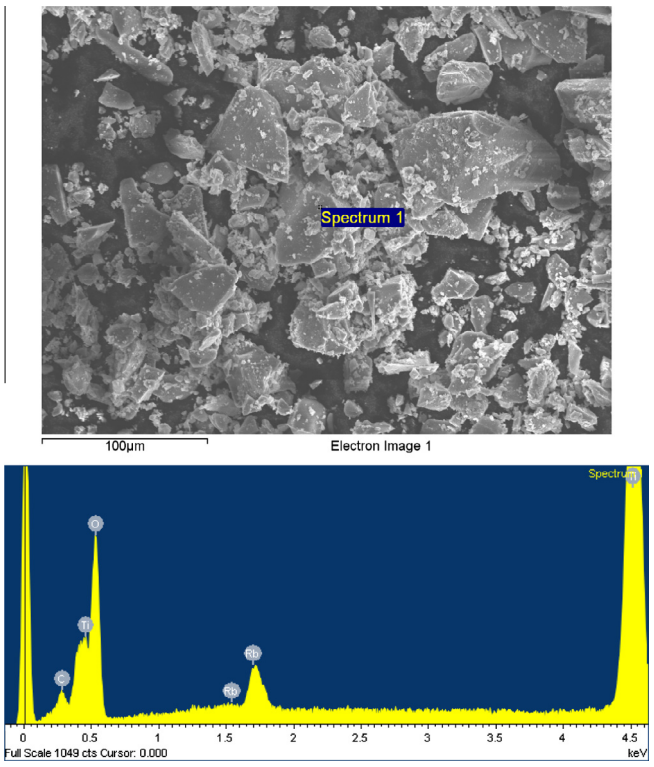

Fig. 6. SEM image and EDX elemental microanalysis of Rb–TiO_2-3% sample.

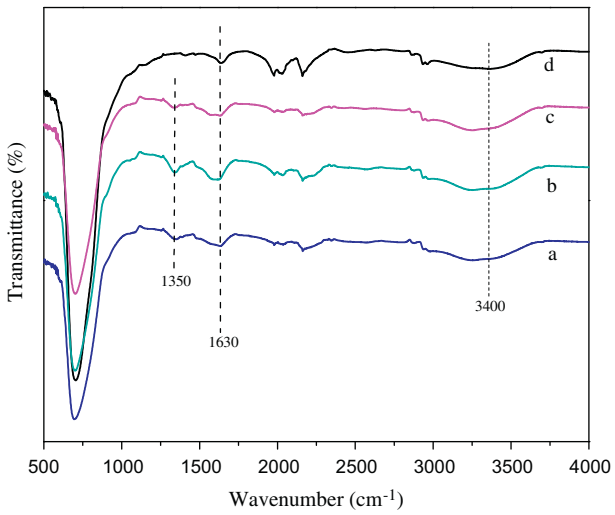

Fig. 7. FT-IR spectra of alkalis doped TiO_2 samples (a) Na–TiO_2-3%, (b) K–TiO_2-3%, (c) Rb–TiO_2-3%, and (d) pure TiO_2.

3.2. Photocatalytic performance

In order to investigate the photocatalytic activity of the alkalis doped TiO_2 samples, the photodegradation experiment was carried out under UV light illumination. Table 1 summarized the catalytic performances for the photodegradation of methyl orange under 60 min irradiation times using the various alkalis doped TiO_2 nanocrystal catalysts. It was reported that MO solution is very stable and does not normally degrade under visible and UV light, except when assisted by an appropriate photocatalyst [14]. The photoreaction results show that the use of the as-prepared alkalis doped TiO_2 photocatalysts and pure reference TiO_2 sample can lead to a decomposition of methyl orange after irradiation under UV-light for 60 min. Table 1 also reveals that the optimal nominal alkali ions doping level for the synthesis of alkalis doped TiO_2 samples with higher photocatalytic activity is 3 wt%. It was seen that the Na–TiO_2-3% catalyst exhibits the highest catalytic activity among all catalysts evaluated, and the MO decomposition rate of Na–TiO_2-3% reaches 77% within 60 min irradiation, which is much faster than that of the reference TiO_2. Furthermore, the K–TiO_2-3% catalysts also show a higher photocatalytic performance in comparison with the pure TiO_2 sample. However, the sample synthesized with 3 wt% Rb^+ ions demonstrates a lower catalytic performance giving 66% MO decomposition efficiency when compared with Na–TiO_2-3% and K–TiO_2-3% samples under the same experimental conditions, but which still has a higher conversion of MO than that of pure TiO_2. The low photoactivity of Rb–TiO_2-3% sample could be explained by the relative lower crystallinity, which is not favorable for the transfer of photoelectrons from bulk to surface, thus decreasing the concentration of the oxidative species, and resulting in a lower activity for the degradation of MO. Thereafter decreasing or increasing the alkalis doping level cannot further increase the photocatalytic activity.

To evaluate the photochemical stability of the catalyst, the repeated experiment for the photodecomposition of methyl orange were performed using Na–TiO_2-3% sample, and the results are shown in Fig. 8. As can be seen that the recycled Na–TiO_2-3% sample show high stability and durability during the decolorized reaction. After 5 cycles of photocatalytic reaction, the activity of Na–TiO_2 has not obvious drops, and the degradation efficiency remaining 75% within 60 min UV light reaction.

On the basis of all of the above results, we can conclude that the 3 wt% alkali ions doping of the anatase phase of TiO_2 are beneficial for the photocatalytic activity. Several main reasons account for the enhanced photocatalysis of the alkalis doped TiO_2 photocatalysts. First, the high activity of the doped catalyst is related to the particle size of TiO_2 nanocrystals. It is well known that the particle sizes play an important role in photoactivity since the smaller crystals offer greater surface area to volume ratios and therefore enrich organic dyes on the surface of alkalis doped TiO_2 [36]. As can be seen from Table 1, all the TiO_2 samples doped with 3 wt% alkalis have much smaller particle size and larger specific surface areas than those of the reference pure TiO_2, and thus increase the surface adsorption of MO molecules and OH groups to participate in the photocatalytic reactions, consequently leading to the improvement of photocatalytic efficiency. Moreover, the crystallinity of alkalis doped TiO_2 materials also plays a vital role in the discolored reaction. From the XRD and Raman analysis (see Figs. 2 and 3), the M–TiO_2-3% samples show the highest crystallinity, this might facilitate the transfer the photoelectrons from bulk to surface and result in the rapid separation of photo-induced electrons and holes, leading to the increased quantum efficiency.

As previously reported [18,37], another reason is that a suitable alkalis doping level has an obvious influence on the concentration of strong basic sites for the photocatalysts modified with Na, K and Rb ions, which was associated to a high photocatalytic activity for the degradation of MO. It was proposed as one of factor, combining TiO_2 with alkali ions can create a large number of basic sites at the surface of the catalyst according to the following reactions: –Ti–O–A → –Ti–O^- + A^+, (A:Na, K and Rb). In the case of our experiments, it was thought that the creation of basic sites at the surface of TiO_2 might benefit for the increased adsorption of the dye molecules and subsequent the electron are injected from its LUMO band to the conduction band of TiO_2 when the system is under irradiation. Thus, the injected electron reacts with the surface-absorbed O_2 to generated active oxygen radicals $O_2^{\cdot-}$. As a consequence, the resultant MO degradation rate is enhanced.

Furthermore, another important effect of alkali ions on the enhanced photocatalytic activity of the catalysts should also be mentioned, which is, the existence of surface alkali ions predominantly as a shallow electron trap could improve electron transfer efficiency from the valence band of TiO_2 to the conduction band of TiO_2, and then the adsorbed oxygen molecules react with conduction band electron to yield superoxide radical anions, which is further transformed to $HO_2^{\cdot}$ and ·OH [25,38], leading to the efficient photooxidation of organic dye under UV light irradiation. From the above discussion, we tentatively concluded that the better photocatalytic activity of alkalis doped TiO_2 samples were relevant to the synergistic effect of pure anatase TiO_2 phase structure, the smaller particle size and the increased transfer efficiency of the electrons, in addition to the well crystalline structure.

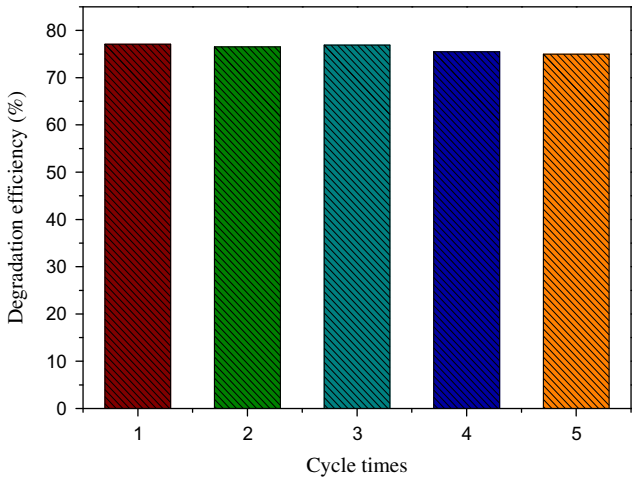

Fig. 8. Recycling testing of the Na–TiO_2-3% sample for degradation of methyl orange under UV light irradiation, reaction time: 60 min.

4. Conclusion

A series of alkalis doped TiO_2 photocatalysts have been successfully prepared via the solovthermal method at low temperature. XRD and Raman analysis results reveal that all of the resultant materials have pure anatase TiO_2 phase. UV–vis diffuse reflectance spectra reveal that the absorption edge of TiO_2 doped with K^+ and Rb^+ leads to a blue shift mainly due to the change of the energy gap of disorder crystal in TiO_2 nanocrystals and the quantum size effects induced by alkalis doping. The photocatalytic activity of the prepared catalysts was evaluated in the reaction of degradation of methyl orange under UV light irradiation. The optimal alkali ions doping level is 3 wt%. Coupling TiO_2 with alkali ions gives rise to a higher decomposition rate of methyl orange with UV light illumination due to the presence of alkali ions promotes the formation of basic sites on surface of TiO_2, which may, as mentioned earlier, increase the photocatalytic activity. In addition, the improvement

in the activity of alkalis doped TiO_2 samples is also related to the high transfer efficiency of photoexcited electron.

Acknowledgements

This work was financially supported by the Fundamental Research Funds for the Central Universities (Grant No. 2012jdhz40). The author would like to thank the UK Photocatalysis Network for their kind support.

Appendix A. Supplementary material

Supplementary data associated with this article can be found, in the online version, at http://dx.doi.org/10.1016/j.jallcom.2013.05.074.

References

[1] D.V. Bavykin, J.M. Friedrich, F.C. Walsh, Adv. Mater. 18 (2006) 2807–2824.
[2] Q. Xiao, L. Gao, J. Alloys Comp. 551 (2013) 286–292.
[3] A. Fujishima, X. Zhang, D.A. Tryk, Surf. Sci. Rep. 63 (2008) 515–582.
[4] F. Han, V.S.R. Kambala, M. Srinivasan, D. Rajarathnam, R. Naidu, Appl. Catal. A: General 359 (2009) 25–40.
[5] B. Liu, L. Peng, J. Alloys Comp. 571 (2013) 145–152.
[6] H.L. Meng, C. Cui, H.L. Shen, D.Y. Liang, Y.Z. Xue, P.G. Li, W.H. Tang, J. Alloys Comp. 527 (2012) 30–35.
[7] T.R. Gordon, M. Cargnello, T. Paik, F. Mangolini, R.T. Weber, P. Fornasiero, C.B. Murray, J. Am. Chem. Soc. 134 (2012) 6751–6761.
[8] J. Du, W. Chen, C. Zhang, Y. Liu, C. Zhao, Y. Dai, Chem. Eng. J. 170 (2011) 53–58.
[9] A.K. Benabbou, Z. Derriche, C. Felix, P. Lejeune, C. Guillard, Appl. Catal. B: Environ. 76 (2007) 257–263.
[10] U. Diebold, Surf. Sci. Rep. 48 (2003) 53–229.
[11] A.L. Linsebigler, G. Lu, J.T. Yates, Chem. Rev. 95 (1995) 735–758.
[12] G. Yang, Z. Jiang, H. Shi, M.O. Jones, T. Xiao, P.P. Edwards, Z. Yan, Appl. catal. B: Environ. 96 (2010) 458–465.
[13] H. Yan, S.T. kochuveedu, L.N. Quan, S.S. Lee, D.H. Kim, J. Alloys Comp. 560 (2013) 20–26.
[14] G. Yang, T. Xiao, J. Sloan, G. Li, Z. Yan, Chem. Eur. J. 17 (2011) 1096–1100.
[15] B. Tian, C. Li, J. Zhang, Chem. Eng. J. 191 (2012) 402–409.
[16] K. Elghniji, A. Atyaoui, S. Livraghi, L. Bousselmi, E. Giamello, M. Ksibi, J. Alloys Comp. 541 (2012) 421–427.
[17] L.-C. Chen, C.-M. Huang, F.-R. Tsai, J. Mol. Catal. A: Chem. 265 (2007) 133–140.
[18] Y. Bessekhouad, D. Robert, J-V. Weber, N. Chaoui, J. Photochem. Photobiol. A: Chem. 167 (2004) 49–57.
[19] T. López, J. Hernandez-Ventura, R. Gómez, F. Tzompantzi, E. Sánchez, X. Bokhimi, A. García, J. Mol. Catal. A: Chem. 167 (2001) 101–107.
[20] S. Bouattour, A.M.B.D. Rego, L.F.V. Ferreira, Mater. Res. Bull. 45 (2010) 818–825.
[21] P. Panagiotopoulou, D.I. Kondarides, J. Catal. 267 (2009) 57–66.
[22] G. Yang, Z. Yan, T. Xiao, Appl. Surf. Sci. 258 (2012) 4016–4022.
[23] Z. Liu, D.D. Sun, P. Guo, J.O. Leckie, Chem. Eur. J. 13 (2007) 1851–1855.
[24] B. Thirupathi, P.G. Smirniotis, Appl. Catal. B: Environ. 110 (2011) 195–206.
[25] G. Yang, Z. Jiang, H. Shi, T. Xiao, Z. Yan, J. Mater. Chem. 20 (2010) 5301–5309.
[26] K.L. Frindell, M.H. Bartl, A. Popitsch, G.D. Stucky, Angew. Chem. Int. Ed. 41 (2002) 959–962.
[27] M.M. Oliveira, D.C. Schnitzler, A.J.G. Zarbin, Chem. Mater. 15 (2003) 1903–1909.
[28] G. Yang, Z. Yan, T. Xiao, Appl. Surf. Sci. 258 (2012) 8704–8712.
[29] M.H. Harunsani, F.E. Oropeza, R.G. Palgrave, R.G. Egdell, Chem. Mater. 22 (2010) 1551–1558.
[30] J.D. Deloach, G. Scarel, C.R. Aita, J. Appl. Phys. 85 (1999) 2377.
[31] G.H. Li, L. Yang, Y.X. Jin, L.D. Zhang, Thin Solid Films 368 (2000) 163–167.
[32] Z.-H. Yuan, C.-C. Tang, S.-S. Fan, Chin. Phys. Lett. 18 (2001) 1520–1522.
[33] F. Fresno, M.D. Hernández-Alonso, D. Tudela, J.M. Coronado, J. Soria, Appl. Catal. B: Environ. 84 (2008) 598–606.
[34] Y. Huo, Y. Jin, J. Zhu, H. Li, Appl. Catal. B Environ. 89 (2009) 543–550.
[35] R. Linker, I. Shmulevich, A. Kenny, A. Shaviv, Chemosphere 61 (2005) 652–658.
[36] X. Chen, X. Wang, Y. Hou, J. Huang, L. Wu, X. Fu, J. Catal. 255 (2008) 59–67.
[37] M. Zamora, T. López, R. Gómez, M. Asomoza, R. Melendrez, Catal. Today. 107–108 (2005) 289–293.
[38] C. Wang, C. Shao, X. Zhang, Y. Liu, Inorg. Chem. 48 (2009) 7261–7268.